Coastal Engineering 136 (2018) 96–105

Contents lists available at ScienceDirect

Coastal Engineering

journal homepage: www.elsevier.com/locate/coastaleng

Nourishment evolution and impacts at four southern California beaches: A sand volume analysis

B.C. Ludka *, R.T. Guza, W.C. O'Reilly

Scripps Institution of Oceanography, University of California, San Diego, United States

ARTICLE INFO

Keywords:
Beach nourishment
Sand replenishment
Beach fill
Nourishment evolution
Observations
Total sand volume estimate
Sand budget
Alongshore transport
Sand spit
Wave-built crown

ABSTRACT

Four southern California beaches were nourished with offshore sand placed as subaerial pads several meters thick, ~50 m wide, and spanning between 500 and 1500 m alongshore. Three nourishments constructed with coarser than native sand, placed in 2012 at Imperial, Cardiff and Solana Beaches, elevated subaerial sand volumes for several years even when exposed to the energetic winter waves of the 2015-16 El Niño, followed by a stormy 2016-17 winter. As these relatively resilient pads were overwashed, landward tilted subaerial profiles (accretionary crowns) formed at the eroding front face of the originally flat-topped pads and pooling occurred in the backbeach. At Imperial Beach, nourishment sand helped prevent waves from directly impacting riprap fronting houses, while groundwater flooding behind the pad was observed at a location where the pad was elevated ~1.6 m above the street. As the nourishments retreated, alongshore oriented spits grew downdrift from the eroding face. The alongshore displacement of the subaerial center of mass of the 2012 nourishments is positively correlated with the seasonally varying S_{xy} (the alongshore radiation stress component). After four years, the net southward drift of the Imperial Beach nourishment contributed to the winter 2016 closure of the Tijuana River mouth and the associated hyper-polluted and anoxic estuary conditions. Nourishment impacts on sand levels on rocky reefs were not unambiguously detectable in the background of natural variability. Over several years, gains or losses in the total sand volume (integrated from the back beach to 8 m depth, over the few km alongshore survey spans) are sometimes comparable to nourishment volumes, suggesting relatively large interannual sediment fluxes across the control volume boundaries. The clearest trend in total volume is at Torrey Pines; during 16 years since the 2001 nourishment, about 300,000 m^3 of sand has been lost. If the trend continues, the thinning veneer of sand will be removed more often from the subaerial winter beach, exposing rocks and cobbles.

1. Introduction

Beach nourishment, placing imported sand to widen and elevate the subaerial beach (Fig. 1), is used to mitigate flooding and erosion, and to promote tourism and recreation. The observations presented here detail the evolution of four nourished southern California beaches. The Torrey Pines nourishment was one of 12 San Diego County sand placement projects in 2001 ($17.5 million total cost). Cardiff, Solana and Imperial Beaches were nourished in 2012, along with five other sites ($28.5 million total cost) (Griggs and Kinsman, 2016). A 50-year, $160 million plan for repetitive beach nourishments in north San Diego County has been developed (Diehl, 2015). Despite the frequency and expense of beach nourishments worldwide (Clayton, 1991; Haddad and Pilkey, 1998; Trembanis and Pilkey, 1998; Valverde et al., 1999; Hanson et al., 2002; Cooke et al., 2012; Luo et al., 2015), the wave-driven redistribution of nourishment sand is rarely monitored in detail and previous studies are limited. Wave conditions are often not observed (Cooper, 1998; Davis et al., 2000; Gares et al., 2006; Benedet et al., 2007; Park et al., 2009; Roberts and Wang, 2012) or are crudely approximated (Kuang et al., 2011). Monitoring schemes may be constrained in temporal resolution (Cooper, 1998; Browder and Dean, 2000; Gares et al., 2006; Benedet et al., 2007; Park et al., 2009; Bocamazo et al., 2011), duration (Elko and Wang, 2007), alongshore span (Anfuso et al., 2001), cross-shore extent (Gares et al., 2006), or by the accuracy of the survey technique (e.g. aerial photography) (Bocamazo et al., 2011). Cost-benefit analysis of beach nourishment impacts, crucial as seas rise (Stocker et al., 2013) and global coastal populations increase (McGranahan et al., 2007), are hindered by a lack of comprehensive observations of waves conditions and sand level evolution. More thorough studies include the well monitored "Sand Engine mega-nourishment" on the Dutch coast (de

* Corresponding author.
E-mail address: bludka@ucsd.edu (B.C. Ludka).

https://doi.org/10.1016/j.coastaleng.2018.02.003
Received 17 June 2017; Received in revised form 10 December 2017; Accepted 7 February 2018
Available online 2 March 2018

Fig. 1. Mechanical sand placement underway, from south to north, at Imperial Beach. Black dots roughly outline the original placement region.

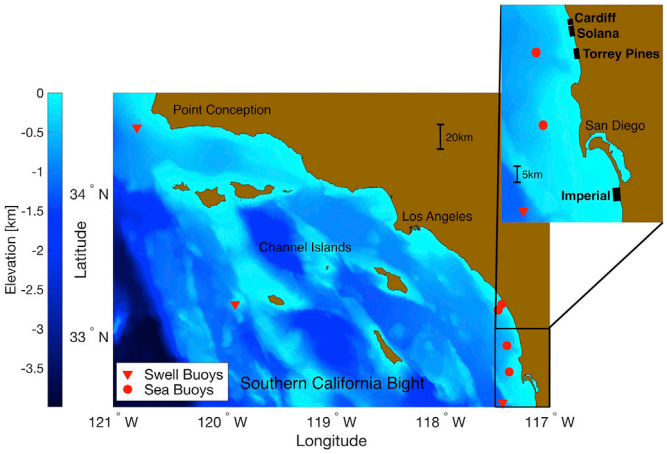

Fig. 2. Map of the southern California Bight, with wave buoy locations (circles are used for local seas, triangles for swell). The inset shows the locations of the study beaches.

Schipper et al., 2016), and the combined impacts of beach nourishment, shore nourishment and a bypassing system on the Gold Coast, Australia (Castelle et al., 2009).

Here, we discuss uniquely detailed sand level observations at four nourished southern California beaches, extending the work of Seymour et al. (2005), Yates et al. (2009) and Ludka et al. (2016). The most recent study (Ludka et al., 2016) considered subaerial sand level observations at these beaches through mid-winter of the erosive 2015-16 El Niño. The present analysis is extended seaward to 8 m depth, and includes recovery of the subaerial beach during summer 2016, followed by the response to the energetic 2016-17 winter (the third most erosive winter during the 16 year monitoring period, ranking behind the 2009-10 and 2015-16 El Niño). Observations of waves and sand levels are described in section 2. Section 3 describes nourishment evolution at Imperial Beach, including pad retreat and accretionary crowns (section 3.1), spit formation and alongshore transport (section 3.2), and nearshore sand volume analysis (section 3.3). Section 4 compares and contrasts nourishment evolution at all sites and includes an investigation of nourishment impacts on sand levels over rocky reefs (section 4.4). Conclusions are summarized in section 5.

2. Observations

2.1. Waves

Swell waves (10–25s) were observed at offshore buoys (triangles, Fig. 2) and propagated shoreward over the complex bathymetry of the Southern California Bight using a spectral refraction model (O'Reilly and Guza, 1998). Island shadowing and local shoals can create sharp spatial gradients, and swell wave heights can vary substantially over less than a few km. A regional wave model, initialized offshore of complex bathymetry, is used to model this spatial structure. In contrast, local sea wave (2–12.5s) heights are usually highly correlated over distances of O (10 km) and are estimated using nearby buoys (circles, Fig. 2). The swell and sea models are combined to estimate hourly directional wave estimates every 100 m alongshore at Monitoring and Prediction (MOP) locations in 10 m depth (O'Reilly et al., 2016). In winter relatively energetic waves arrive from the north, and in summer milder waves come from the south. With roughly N-S study beach orientations (Fig. 2 inset), the radiation stress component S_{xy} has strong seasonal variation.

2.2. Sand levels

Monitoring at each of the 4 individual nourishment sites spans between 1.7 and 4.1 km alongshore and 8–16 years. Quarterly bathymetric surveys from the backbeach to 8 m depth were performed on cross-shore transects spaced 100 m apart. A few surveys had finer alongshore resolution; 20 m at Torrey Pines centered on the nourishment placement, and 50 m at Cardiff. Monthly subaerial elevation surveys were on shore-parallel tracks spaced ~10 m in the cross-shore. Surveys are mapped to a coastline following grid (Appendix A). During monitoring, each beach was nourished with between 68,000–344,000 m^3 of sand, over subaerial alongshore spans between 500 and 1 500 m (Table 1). Imperial Beach was the largest nourishment, had controversial impacts (Hargrove, 2015; Baker, 2016), and is described in the most detail. Additional results for other sites are in Supplementary Material.

3. Nourishment evolution at Imperial Beach

In September of 2012, 344,000 m^2 of relatively coarse grained sand (compared to native, Table 1) was mechanically placed at Imperial Beach (Fig. 1). Much of the nourishment sand remained subaerial for several

Table 1
Nourishment statistics.

Beach	Native Grain Size [mm][a]	Nourishment Grain Size [mm][b]	Nourishment Volume [m^3][c]	Subaerial Survey Area [m^2]	Jumbo Survey Area [m^2]
Torrey	0.23	0.2	187,000	171,715	1,094,546
Imperial	0.25	0.53	344,000	252,358	1,610,518
Cardiff	0.16	0.57	68,000	95,499	629,437
Solana	0.15	0.55	107,000	104,968	1,213,960

[a] D_{50} at MSL. Torrey, Imperial and Cardiff from Ludka et al. (2015). Solana from Group Delta Consultants (1998).
[b] D_{50}. Torrey from Seymour et al. (2005). Imperial, Cardiff, and Solana from Coastal Frontiers (2015).
[c] Coastal Frontiers (2005, 2015).

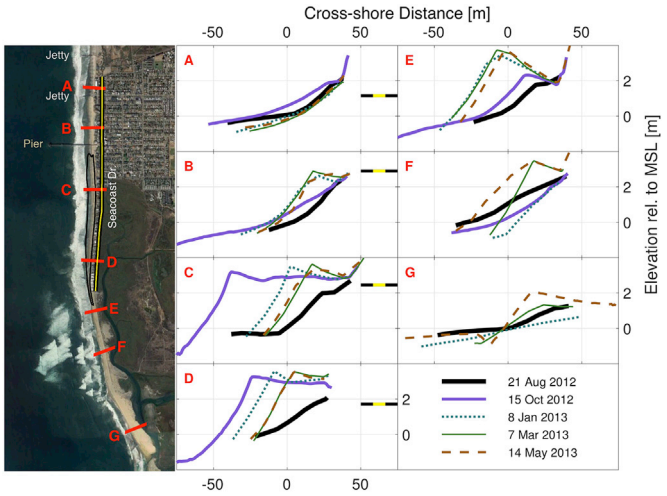

Fig. 3. (Left) Satellite image of Imperial Beach. Original nourishment region outlined in black. Seacoast Drive highlighted as black and yellow lines. (A–G) Cross-shore profiles at Imperial Beach relative to mean sea level (MSL). Panels correspond to red transects on left map and dates plotted correspond to legend in bottom right. Seacoast Drive elevations (located with LIDAR) at x = 100m±30 m are shown as black and yellow dashed lines on the right in panels A–D. (For interpretation of the references to color in this figure legend, the reader is referred to the Web version of this article.)

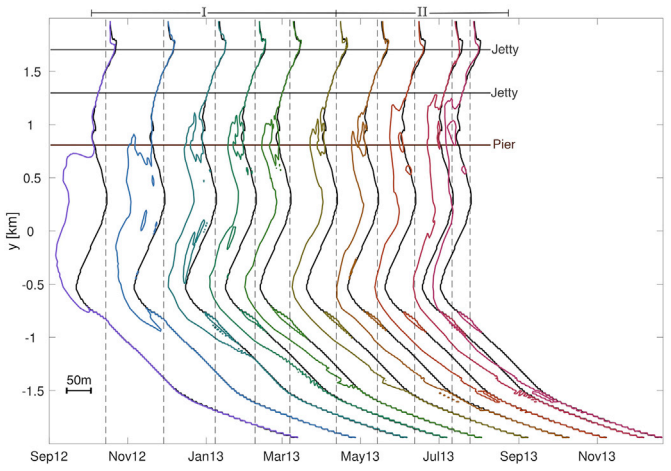

Fig. 5. Horizontal location of 2.5 subaerial depth contour versus time at Imperial Beach. The black curve, showing repeatedly, is prenourishment (21 Aug 2012). Time periods I and II are labeled.

years after placement (Ludka et al., 2016).

3.1. Pad retreat and accretionary crowns

As the originally flat-topped nourishment pad retreated, overtopping waves formed an accretionary crown at the seaward berm edge, and the pad edge became increasingly elevated (Fig. 3C-D). Crowns were sometimes formed, destroyed and reformed, and in some instances multiple crowns were observed on a profile (Fig. 4D, Nov 2015, in Ludka et al. (2016)). The landward sloping nourishment pad at Imperial Beach was backed by riprap, fronting houses. At high tide, waves sometimes overtopped the berm (Fig. 4a). Without the residual nourishment berm, waves would have impacted directly onto the riprap. At low tide, surface water pooled in the low region behind the accretionary crown (Fig. 4b). The + 3 m pad elevation was ~1.6 m above the elevation of the street backing the southern nourishment pad (Fig. 3D), and ground water from below flooded garages (Hargrove, 2015) and emerged through the sidewalk.

3.2. Spit formation and alongshore transport

As the nourishment pad narrowed in the cross-shore, it stretched alongshore. Sequential plan views of the 2.5 m contour elevation during the year following nourishment show the growth of alongshore oriented spits originating at the eroding pad face (Fig. 5). Spit growth also caused landward sloping cross-shore profiles adjacent to the region of original nourishment placement (Fig. 3B,E,F,G). While spits emerged from both pad ends during the first few months after nourishment, growth was predominantly southward during the winter after placement (phase I, Fig. 5). Afterwards, summer spit growth protruded northward to a jetty which may have impeded further subaerial transport (phase II, Fig. 5). The spring after nourishment placement, we collected and analyzed 106 subaerial sand samples in Imperial Beach and south several km into Mexico. While we were able to identify the northward extent of nourishment propagation, we were unable to unambiguously track nourishment sand by grain size near the river mouth (Supporting material Figure S1).

The alongshore transport and spreading of nourishment sand at Imperial Beach (Fig. 6) is quantified using the volume of subaerial sand-in-play $V_{sub}(t)$

$$V_{sub}(t) = \int_{A_{sub}} [h(x,y,t) - h_{min}(x,y)]da \quad (1)$$

where $h_{min}(x,y)$ is the minimum observed elevation surface (Appendix A, Figure A1), and the integral is over the subaerial area A_{sub}, extending cross-shore from the offshore location with average elevation, $< z >=$ -0.5 m, to the backbeach, and alongshore over the survey span.

The center of mass (black x's, Fig. 6) of $V_{sub}(t)$ is at alongshore location $\tilde{y}_{com}(t)$ where

$$\tilde{y}_{com}(t) = \frac{1}{V_{sub}(t)} \int_{A_{sub}} \tilde{y}(x,y)[h(x,y,t) - h_{min}(x,y)]da \quad (2)$$

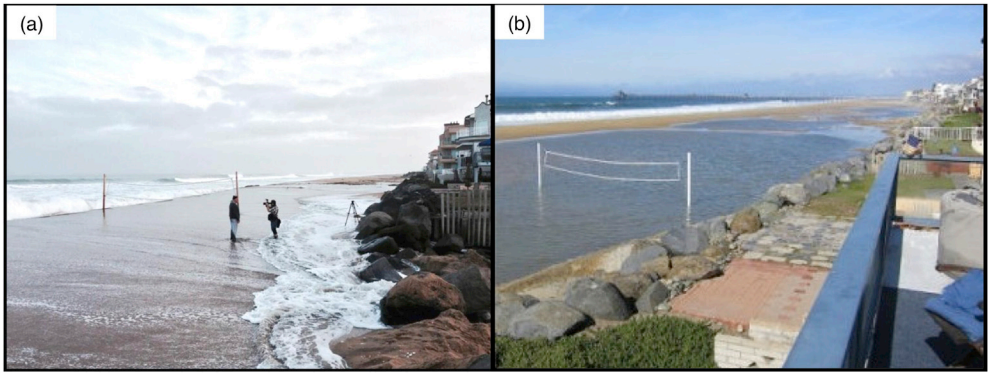

Fig. 4. Photos of Imperial Beach at location D from Fig. 3. (a) Landward tipping nourishment pad at high tide on 30 January 2014. (b) Water pooling on the backbeach nourishment pad at low tide on 23 January 2013 (Hargrove, 2015).

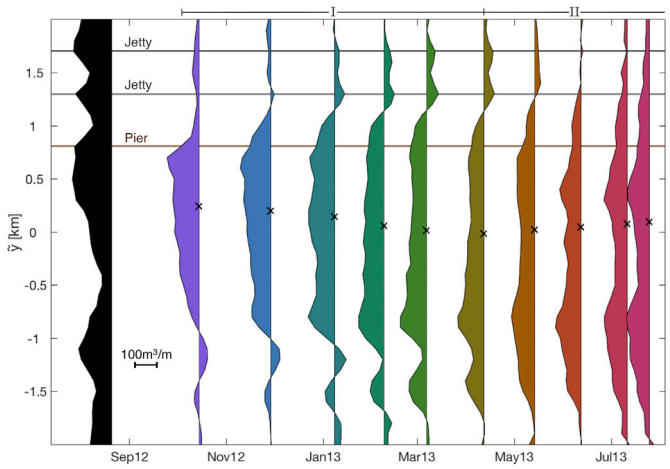

Fig. 6. Subaerial sand-in-play (above the minimum surface) versus alongshore location ỹ and time at Imperial Beach. To highlight the nourishment, prenourishment volume (21 Aug 2012, black) is subtracted from later times. Time periods I and II are labeled. The black x indicates the subaerial center of mass $\tilde{y}_{com}$ (Equation (2), Fig. 8b).

Table 2
Coastline orientation and wave direction.

Beach	Mean (Min:Max) Coastline Orientation [degrees][a]	Std Dev Coastline Orientation [degrees][a]	Mean Wave Direction [degrees][b]	Std Dev Wave Direction [degrees][b]
Imperial	264 (246:275)	10	**265**	**6**
Phase I			267	3
Phase II			262	8
Cardiff	259 (244:267)	7	**255**	**8**
Phase I			260	5
Phase II			253	10
Solana	256 (241:266)	7	**258**	**8**
Phase I			262	5
Phase II			256	10

[a] Derived from MOP line locations (O'Reilly et al., 2016). Mean is alongshore average. Std Dev is standard deviation alongshore.

[b] Alongshore averaged wave direction in 10 m depth at MOP locations (O'Reilly et al., 2016). Means are time averaged (over Phases I, or II), and Std Dev is the standard deviation. Bold indicates an average over the entire record.

During the winter following nourishment (November 2012–May 2013), $\tilde{y}_{com}$ drifted south (phase I, Fig. 6), followed by a smaller northward drift the subsequent summer (phase II, Fig. 6). On average, waves were more northerly during phase I, and more southerly during phase II (Table 2).

3.3. Nearshore sand volumes

The total volume of sand-in-play, $V_{tot}(t)$ (Fig. 7c, integrated from the backbeach to 8 m depth and over the entire survey area A_{tot}),

$$V_{tot}(t) = \int_{A_{tot}} [h(x,y,t) - h_{min}(x,y)]\, da \tag{3}$$

shows that nourishment increased $V_{tot}(t)$ at Imperial Beach by ~380,000 m^3 (Fig. 7c). The difference with the design volume of 344,000 m^3 (Table 1) is smaller than estimated measurement errors (Appendix B). As of July 2016 (last profile survey in Fig. 7c) ~ 1/2 of the nourishment sand remains in the survey area. Volumes divided into cross-shore regions show that the bulk of the observed retained sand remained subaerial (Fig. 7d), despite energetic winter waves during both 2015-16 (El Niño, (Ludka et al., 2016)) and 2016-17 (Fig. 7b). These waves were significantly larger than the storm (black dotted line, Fig. 7b) that washed the entire 2001 nourishment pad (constructed with a grain size similar to native, Table 1) offshore at Torrey Pines (Seymour et al., 2005).

Subaerial sand levels at Imperial Beach increased at all alongshore sections after nourishment (Fig. 7e), with a net southward drift of nourishment sand propagation from C to D, and then from D to E. In the last survey, 3.5 yrs and an El Niño after nourishment, regions D and E combined contain ~50,000 m^3 more sediment than pre-nourishment (about 70% the Cardiff nourishment design volume of 68,000 m^3, Table 1). The Tijuana River, the southern border of region E, clogged in April 2016 (blue star above Fig. 7b), causing hyper-polluted and anoxic conditions in the estuary (Baker, 2016). The blockage was mechanically removed (Fig. 7f). The last previous closure was during a strong 1983 El Niño, when there was no nourishment. El Niño conditions and the nourishment likely both contributed to closure in April 2016.

4. Intersite comparison

4.1. Pad retreat and accretionary crowns

Accretionary crowns formed in the original placement region on all of the relatively coarse grained nourishments (Imperial, Cardiff and Solana Beaches, Table 1, Figs. S2B–D). Crowns were not observed in the original placement region at Torrey Pines (Fig. S2A), as the pad, constructed with a grain size similar to native (Table 1), was not overtopped until the storm of 22 November 2001, when the entire nourishment washed offshore (Seymour et al., 2005). The wave and sand mechanics underlying crown formation are not understood, but they form and evolve with small to moderate pad overwash and retreat.

4.2. Spit formation and alongshore transport

At all sites, including Torrey Pines, landward sloping subaerial profiles formed adjacent to the original nourishment pads as the surrounding beach accreted seaward (Figs. S2E–H). Sequential plan views of contour elevations on the upper beach (e.g. 1.5 or 2.5 m contours in Fig. S3) during the year following nourishment show that the increasingly landward sloping profiles adjacent to the placement region are associated with growth of alongshore oriented spits originating at the eroding pad face. Elko and Wang (2007) suggest smooth end transitions may minimize spit formation, but spits were not suppressed by the slightly tapered edges of the constructed nourishments (Fig. 1) (Moffatt and Nichol, 2013).

As the nourishment pads elongated, the alongshore spread of the volume of subaerial sand-in-play (Equation (1)),

$$\sigma_y(t) = \sqrt{\frac{1}{V_{sub}} \int_{A_{sub}} [\tilde{y}(x,y) - \tilde{y}_{com}(t)]^2\, [h(x,y,t) - h_{min}(x,y)] da}. \tag{4}$$

generally increased over time, although cross-shore transport (non-conservation of V_{sub}) likely caused spread to occasionally decrease with increasing time (Fig. 8a, where Torrey Pines is not shown because nourishment sand only remained subaerial for a summer season, Fig. S4a, (Seymour et al., 2005)).

During the winter and spring (November 2012–May 2013) following nourishment at Imperial, Cardiff and Solana Beaches, $\tilde{y}_{com}$ (Equation (2)) drifted south (black x's, phase I, Figs. S4b–d), followed by a smaller northward drift the following summer (black x's, phase II, Figs. S4b–d). Seasonal up- and down-coast migration of $\tilde{y}_{com}$ continued for several years at Imperial and Solana beaches (Fig. 8b). At Torrey Pines the nourishment pad remained subaerial for only one summer, not long enough to observe reversals.

The alongshore velocity of $\tilde{y}_{com}$ ($d\tilde{y}_{com}/dt$, Fig. 8c) and the alongshore component of the radiation stress S_{xy} (Fig. 8d) (Longuet-Higgins, 1970; Thornton and Guza, 1986) are significantly correlated (R^2 ~ 0.5, Fig. 8e). At the three 2012 nourishments, $d\tilde{y}_{com}/dt$ and S_{xy} vary seasonally

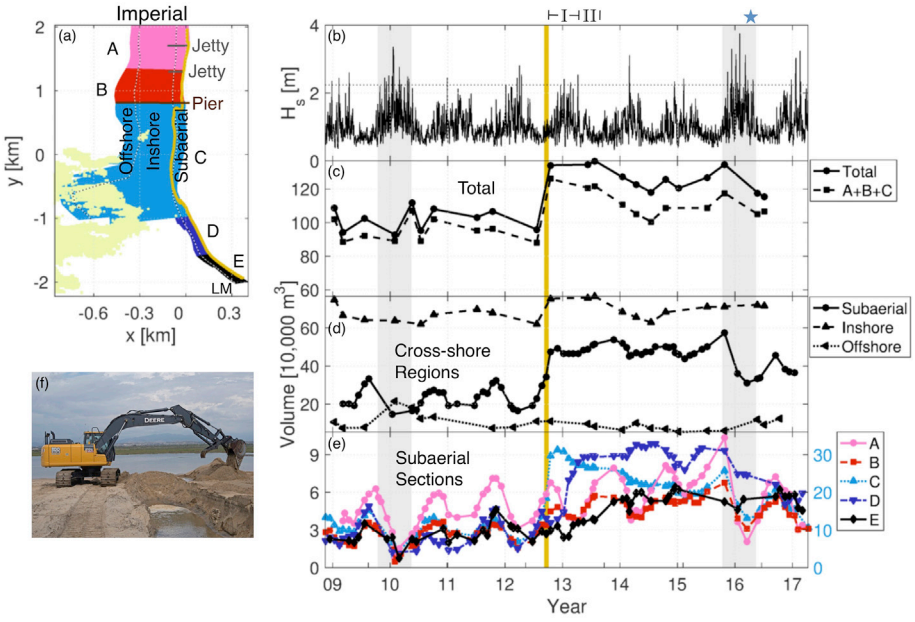

Fig. 7. Imperial Beach. (a) Map of subareas. Cross-shore regions are defined by the location of time averaged (excluding nourishments) depth contours. Regions are, relative to MSL; subaerial (backbeach to −0.5 m), inshore (−0.5 to −6.5 m), and offshore (−6.5 to -8 m). Yellow indicates a cobble shoal identified with a sidescan survey in Moffatt and Nichol (2009). Gold line indicates post-nourishment 2.5 contour location from Fig. 5. The Tijuana lagoon mouth is labeled LM. (b) Daily averaged significant wave height. (c–e) Subarea volumes versus time; (c) total (all subareas), (d) cross-shore regions, and (e) subaerial sections. Note the axis for region C is on the right for panel (e). The southward drift of nourishment sand to subaerial sections D and E preceded (f) Tijuana River mouth dredging on April 11, 2016, labeled with blue star above panel (b). (For interpretation of the references to color in this figure legend, the reader is referred to the Web version of this article.)

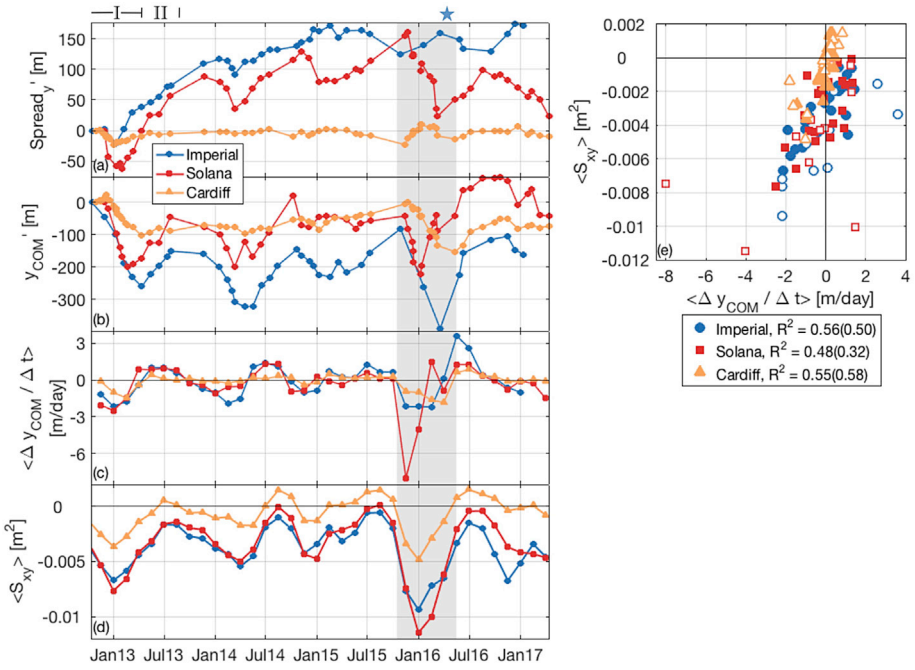

Fig. 8. Time series investigating alongshore transport at Imperial, Solana and Cardiff beaches. (a) Alongshore spread (Equation (4)) about subaerial center of mass of sand in play. (b) Alongshore location of the subaerial center of mass of sand in play $\tilde{y}_{com}$ (Equation (2)), relative to pre-nourishment location. (c) Three month running mean of $d\tilde{y}_{com}/dt$, speed of $\tilde{y}_{com}$. (d) Three month running mean of alongshore radiation stress S_{xy} in 10 m depth, averaged alongshore over each survey region. Shading indicates energetic El Niño winter. (e) S_{xy} versus $d\tilde{y}_{com}/dt$ (from (c) and (d), respectively). R^2 is lower when El Niño and post-El Niño data (open symbols) is included (parentheses in legend). Subaerial maps used in the calculations have alongshore resolution $\Delta\tilde{y}$ = 20 m and have less than 10% of values with NMSE>0.2 (Appendix A). Changes of 3° in shoreline orientation would offset each S_{xy} (d) vertically by ~0.002 m^2. Time periods I, and II are indicated.

(Fig. 8c–d), consistent with transport in the direction of the prevailing surfzone current. The velocity $d\tilde{y}_{com}/dt$ is similarly correlated (not shown) with $E^{1/4}S_{xy}$ in 10 m depth, a quantity proportional to the empirical total alongshore transport (e.g. surfzone integrated) (CERC, 1984). The interpretation of the correlation between S_{xy} and $d\tilde{y}_{com}/dt$ as alongshore transport of the nourishment is ambiguous because $\tilde{y}_{com}$ can migrate owing to alongshore variation in cross-shore transport, even in the absence of alongshore transport. V_{sub} is not conserved (e.g. solid black, Fig. 7d) because in winter subaerial sand is moved offshore. On a beach with alongshore variation in the seasonal subaerial volume fluctuations (e.g. Fig. 7e), say owing to different seasonal alongshore variations in wave height, $\tilde{y}_{com}$ moves toward the most rapidly accreting (or most slowly eroding) reach of beach. Along- and cross-shore transport could both contribute to the observed $d\tilde{y}_{com}/dt$.

Using the framework of Pelnard-Considére (1956), Dean (2002) analytically predicts that a rectangular beach nourishment on a straight coast subject to low angle wave conditions will diffuse symmetrically. Dean and Yoo (1992) use a one-line model that assumes all contours from the backbeach to the depth of closure are equally perturbed seaward by the nourishment and recreate the symmetric diffusion scenario of Pelnard-Considére (1956) and Dean (2002) for a nourishment constructed with a grain size similar to native. For a nourishment constructed with a grain size coarser than native, the model of Dean and Yoo (1992) predicts that the coarser sand acts as an erodible barrier to the alongshore transport of native sand, such that $\tilde{y}_{com}$ moves opposite to the longshore current.

The 2012 nourishments were exposed to waves that were typically less than 10° from normal incidence, but with a seasonally varying

preferred quadrant (Table 2). While the associated wave-driven alongshore currents were likely not typically strong, they were persistent. These nourishments, constructed with a grain size coarser than native, evolved asymmetrically, elongating in the direction of the seasonally shifting alongshore currents, opposite the prediction of Dean and Yoo (1992). Over several years, the alternating up- and down-coast transport increased the nourishment spreading. In contrast, the originally asymmetric Dutch mega-nourishment evolved to a symmetric shape in a wave climate with highly oblique waves approaching the beach from both offshore quadrants in all seasons (de Schipper et al., 2016). Castelle et al. (2009) deduced that bypassed sand on the Australian Gold Coast was advected in the direction of the alongshore current.

4.3. Nearshore sand volumes

A simple 1-D beach state model (Ludka et al., 2015) based on an equilibrium hypothesis (Wright and Short, 1984; Wright et al., 1985) is driven with hourly wave energy alongshore averaged across the survey regions at each site, and over all sites. The model, previously calibrated on these beaches, characterizes the cross-shore transport potential of the observed waves on an unnourished beach (Fig. 9a, positive values correspond to accreted subaerial beaches). The volume of subaerial sand-in-play, $V_{sub}(t)$, divided by the subaerial survey area, A_{sub}, yields an average thickness of subaerial sand-in-play (Fig. 9b). The observed seasonal thickness fluctuations and severe subaerial erosion in El Niño winters 2009-10 and 2015-16 correspond qualitatively with beach state. During the 16 year period, subaerial erosion potential was greatest for the El Niño winters of 2009–10 and 2015-16, followed by the 2016-17 winter (Fig. 9a). After the exceptionally energetic 2015-16 El Niño, all four sites recovered (Fig. 9b). Torrey Pines, unnourished since 2001, had a 2016 summer maximum that was lower than all previous 15 summers, continuing the oscillating and thinning trend. Imperial, Cardiff and Solana, nourished in 2012, recovered to a summer maximum thicker than ever observed pre-nourishment. The subsequent 2016-17 winter caused significantly low subaerial sand levels at Torrey Pines, while the sites nourished in 2012 still remained buffered by nourishment compared to erosive winters experienced pre-nourishment. These coarse-grained nourishments were detectable as subaerial superelevations more than 3 yrs after nourishment (movies of super-elevation in supporting material). This juxtaposes the evolution of the 2001 Torrey Pines nourishment, constructed with a grain size similar to native, where the pad completely washed offshore in a single unexceptional storm (red dot, Fig. 10b) (Seymour et al., 2005), partially returning to the upper beach in subsequent summers (Yates et al., 2009).

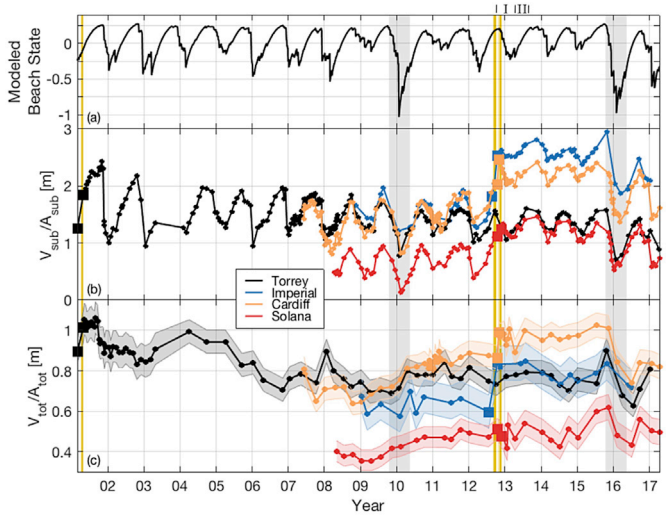

Fig. 9. (a) Modeled beach state (Ludka et al., 2015). (b) Subaerial (Equation (1)) and (c) total volume of sand-in-play (Equation (3)) (normalized by surface area) versus time at four beaches (legend). Subaerial regions (mean elevation > −0.5 m MSL) are outlined in black in Figure A1, and are the regions consistently measured in monthly subaerial surveys. Pre- and post-nourishment surveys (big squares) bracketed each nourishment. Gold shading shows period of nourishment placement. Gray shading indicates energetic El Niño winter. Error bars in (c) are from Appendix B. Surveys where more than 10% of the map has NMSE>0.2 are not plotted (Appendix A). Alongshore resolution in (b) is 20 m for subaerial surveys, whereas full surveys in (c) use $\Delta\tilde{y} = 100$ m at Imperial and Solana Beach, 50 m at Cardiff, and 20 m at Torrey Pines. Time periods I, and II are indicated. (For interpretation of the references to color in this figure legend, the reader is referred to the Web version of this article.)

In contrast to the subaerial $V_{sub}(t)$, the total volume of sand-in-play, $V_{tot}(t)$, (Fig. 9c, integrated from the backbeach to 8 m depth and over the entire survey area A_{tot}), divided by A_{tot} for comparison across sites, does not show strong seasonality because sand exchanged between the subaerial beach and immediately offshore approximately balance. $V_{tot}(t)$, calculated from profile surveys that are more labor intensive and less frequent than subaerial surveys, puts nourishment sand volumes in a spatially larger context. Error estimates (Appendix B) aid in interpreting results. Although subaerial volumes $V_{sub}(t)$ increase during nourishment (Fig. 9b), at Solana Beach $V_{tot}(t)$ decreases between pre and post nourishment surveys. The expected $V_{tot}(t)$ increase due to nourishment at Solana is smaller than the estimated measurement error so may be obscured by noise, or partially balanced by losses elsewhere. Total volume changes are sometimes larger than nourishments and noise, suggesting relatively large net fluxes across the control volume boundaries. At each beach, the largest seasonal $V_{tot}(t)$ change is erosion during the 2015-16 El Niño where the winter $V_{sub}(t)$ minimum precedes the $V_{tot}(t)$ minimum by about 6 months. The cause of the lead is unknown.

Trends are difficult to detect at Cardiff, Imperial, and Solana Beaches because the records are relatively short (8–10yr), with nourishments midway through the time series (Fig. 9). The 16-yr long $V_{tot}(t)$ trend at Torrey Pines, last nourished in 2001, suggests an overall loss of about 300,000 m^3, about 20,000 m^3/yr (Fig. 10c). Distributed over the survey area, the loss is 1.7 cm (+-0.3 cm)/yr. If the trend continues, by mid-century the survey region will erode to the minimum surface, which is at least partially rocky reef offshore and cobbles onshore. Sandy portions of the present minimum surface could be mobilized, reaching new minima. In any case, with a wave-driven (Fig. 10b) seasonal exchange cross-shore (Fig. 10d), the thinning veneer of sand will more often erode the subaerial winter beach (Fig. 10e) to cobbles (Fig. 10g).

At Torrey Pines, between April 2008 and Sept 2016, about 238,000 m^3 of material was dredged from the Los Peñasquitos lagoon (LM in Fig. 10a) and placed on the subaerial beach. The amount of new, sand-sized material added to the Torrey Pines $V_{tot}(t)$ from upland drainage is unknown. Small, dredging related transients can be detected in profiles near the mouth (not shown). The dredged material is placed within a few 100 m of the mouth, where some is transported back into the lagoon, and redredged.

4.4. Sand levels on reefs

Rocky reefs at Cardiff, Solana and Torrey Pines (Fig. 11a), were defined as surfaces not eroding to the levels of the adjacent sandy areas (Figure A1). Between 50 and 100% of reef is buried at any given time (Fig. 11b). Sand cover at Torrey Pines north reef is maximum (100% buried) during the El Niño winters of 2009–10 and 2015-16 (Fig. 10f). The maximum sand thickness at Cardiff south reef in winter 2013 could have been influenced by nourishment sand, but is comparable to other maxima (Fig. 11c). Nourishment impacts on reef sand levels are not unambiguously detectable in the background of natural variability (Figs. 10f, 11, Figs. S5f, S6f).

5. Conclusions

Four southern California beaches received between

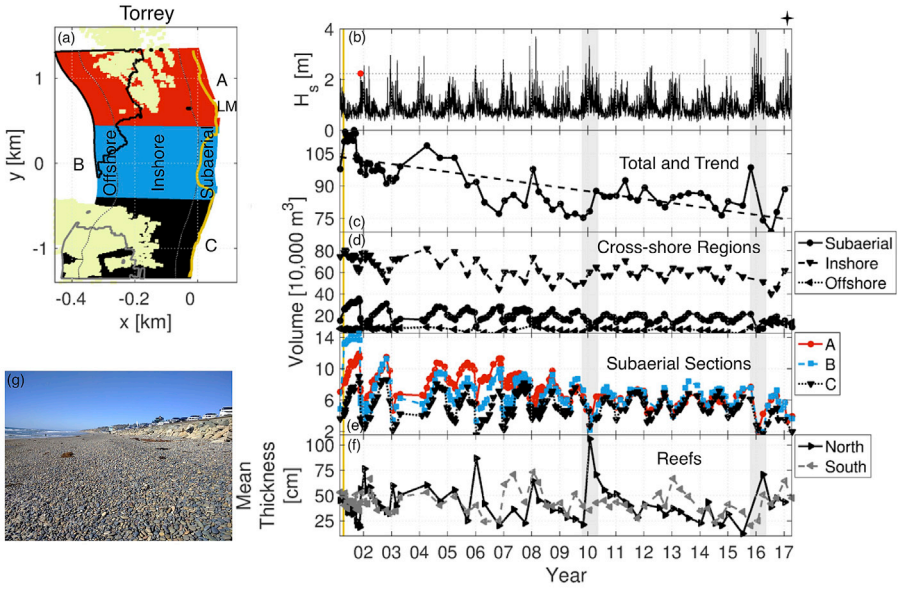

Fig. 10. Torrey Pines Beach. (a) Map of subareas. Cross-shore regions are defined as in Fig. 7 caption. Gold line indicates post-nourishment 1.5 contour location from Fig. S3. Reefs identified using minimum surfaces (Figure A1) are outlined in black and gray. Yellow corresponds to the reefs identified with a sidescan survey in Moffatt and Nichol (2009). The Los Penasquitos lagoon mouth is labeled LM. (b) Daily averaged significant wave height. (c–e) Subarea volumes relative to minimum surface versus time; (c) total (all subareas) and trend (dashed), (d) cross-shore regions, and (e) subaerial sections. (f) Mean sand thickness over reef areas in (a). Gold shading shows period of nourishment placement. Gray shading indicates energetic El Niño winter. (g) Cobble beach on 22 February 2017 (labeled with 4-point star above (b)), where the field of view includes the subaerial northern part of B and southern part of A in (a). (For interpretation of the references to color in this figure legend, the reader is referred to the Web version of this article.)

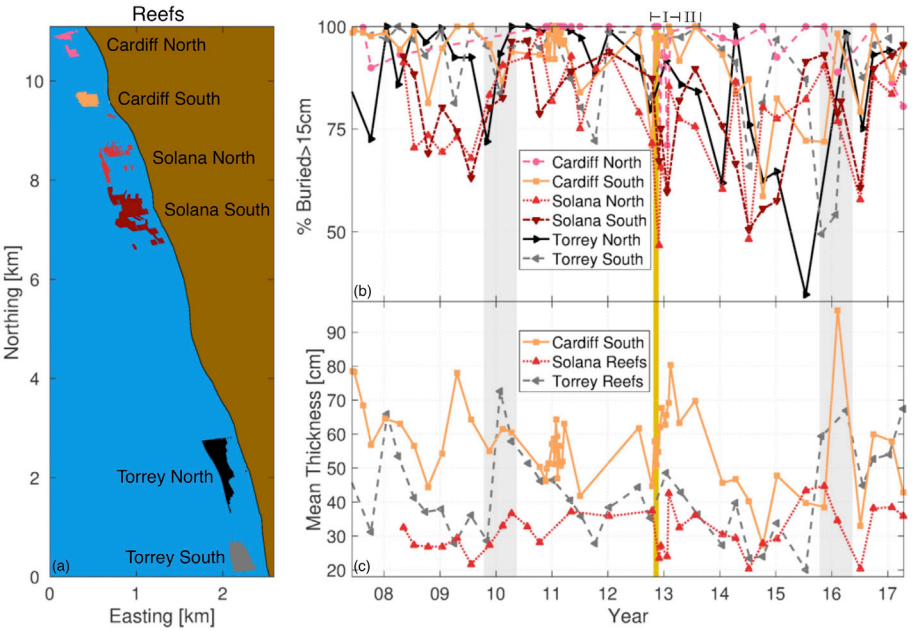

Fig. 11. (a) Plan view of reefs. (b) percent of each reef buried (more than 15 cm) versus time, and (c) mean sand thickness versus time.

68,000–344,000 m^3 of imported sand placed as several meter thick subaerial pads spanning 500–1500 m. The nourishment at Torrey Pines, constructed in 2001 with a sand grain size similar to native, washed offshore during a storm with an unexceptional significant wave height (2.2 m daily average) (Seymour et al., 2005). Imperial, Cardiff and Solana Beaches received relatively coarse-grained sand in 2012 that largely remained subaerial for several years when exposed to wave conditions more energetic than the storm that eroded the pad at Torrey Pines (Ludka et al., 2016). After the extremely energetic storms of the 2015-16 El Niño, all four sites recovered. The subsequent energetic 2016-17 winter caused substantially low subaerial sand levels at Torrey Pines while the sites nourished with coarse sand in 2012 remained buffered by nourishment compared to previously erosive winters pre-nourishment.

As the relatively hardy coarse-grained nourishment pads retreated, an accretionary crown formed on their seaward edge, tilting the originally flat-topped pad landward; the seaward edge of the pad became increasingly more elevated than the backbeach. Spits extending alongshore from the seaward ends of the nourishment pads also created landward sloping subaerial profiles in the regions adjacent to nourishment, similar to the observations of Elko and Wang (2007). The spits elongated asymmetrically, and the subaerial center of mass moved in the direction of the seasonally shifting alongshore currents.

Over several years, gains or losses in the total sand volume (integrated from the back beach to 8 m depth, over the entire alongshore survey spans) are sometimes comparable to nourishment volumes, suggesting relatively large interannual sediment fluxes across the control volume boundaries. If the 16 year erosive trend of ~2 cm/yr at Torrey Pines continues, the thin (<1 m, Fig. 9c) veneer of sand will often leave the subaerial beach eroded down to cobbles. Nourishment impacts on sand levels on rocky reefs were not unambiguously detectable in the background of natural variability.

Cost-benefit analysis of beach nourishments is complex. For low-lying

homes at Imperial Beach, nourishment sand mitigated flooding by wave overtopping but elevated the water table, inducing groundwater flooding (Hargrove, 2015). Nourishment sand affected intertidal invertebrate populations (often negatively) (Wooldridge et al., 2016) and contributed to the clogging of the Tijuana River mouth that created hyper-polluted and anoxic conditions in the estuary (Baker, 2016). In the face of rising seas, limited sand resources (Roelvink, 2015), and increasing coastal populations, detailed monitoring of often expensive beach nourishments provides crucial information for coastal managers attempting to protect coastal infrastructure and maintain thriving tourist economies (Pendleton et al., 2011; WorleyParsons, 2013; Alexandrakis et al., 2015).

Acknowledgments

Support from the United States Army Corps of Engineers (grant number: W912HZ-14-2-0025), the California Department of Parks and Recreation, Division of Boating and Waterways Oceanography Program (grant number: C1370032) (program manager R. Flick), and the Scripps Center for Climate Change Impacts and Adaptation (CCCIA) is gratefully acknowledged. B. Ludka was partially supported by a National Science Foundation Graduate Research Fellowship, NOAA grant NA10OAR4170060, California Sea grant project #R/RCC-01, through NOAAs National Sea Grant College Program, and the NOAA/Southern California Coastal Ocean and Observing System. The statements, findings, conclusions and recommendations are those of the authors and do not necessarily reflect the views of the supporting organizations. B. Woodward, K. Smith, B. Boyd, R. Grenzeback, G. Boyd, and L. Parry built, operated and maintained the surveying system. Captain R. Stabenow (Imperial Beach Lifeguard Captain), and K. Weldon (City of Encinitas Shoreline Management Division Manager) facilitated field work. K. Ritzman (Scripps Assistant Director) and M. Okihiro (Scripps) were essential to maintaining funding and survey continuity. The article was improved by helpful conversations with Bas Huisman, Matthieu de Schipper, Sierd de Vries, and Meagan Wengrove. This article is a reprint with modifications of Chapter 4 of B. Ludka's doctoral thesis.

Appendix A. Coastline following coordinates and mapping

The coastline following coordinate systems, based on surveys without measurable influence of beach nourishment, use surveys before the fall 2012 nourishment placements at Imperial, Cardiff and Solana beaches, and (somewhat arbitrarily), all surveys after Jan 7, 2004 at Torrey Pines. MOP lines, extending from backbeach locations spaced 100 m apart in the alongshore, to the nearest offshore location on the 10 m bathymetric contour, are used as the alongshore coordinate, $\tilde{y}$. Transect lines at Imperial and Solana beach are aligned with the MOP lines, as well as the surveys after 31 October 2011 at Cardiff beach. Only the bathymetric surveys with transects aligned with MOP lines were used to calculate the coastline following coordinate system at Cardiff. The mean horizontal positions of contours spaced 15 cm in the vertical, are used as the cross-shore coordinate, $\tilde{x}$. These horizontal positions were extracted from interpolated profiles along the predetermined transect lines. Profiles from quarterly bathymetric surveys were created by bin-averaging elevations in 20 m alongshore by 1 m cross-shore bins centered on the transect lines, applying a 2 m cross-shore moving average, and splining to a 1 m grid wherever breaks in the data do not exceed 20 m. Subaerial profiles from the monthly beach surveys were created using a Delaunay triangulation linear interpolation of observations within 20 m wide alongshore swaths centered on transect lines. At Torrey Pines, transect lines are not aligned with MOP lines, so the mean horizontal contour locations were linearly interpolated to MOP lines.

Survey data were binned in grid cells defined in coastline following coordinates. At Imperial and Solana Beaches, full survey grid cells were 100 m $\Delta\tilde{y}$ apart, centered on MOP lines, and cross-shore bins were spaced $\Delta\tilde{x}$ such that mean vertical elevations varied by 15 cm. Because of the sometimes higher alongshore resolution bathymetry surveys at Cardiff and Torrey Pines Beach, these observations were instead binned to grid cells with 50 m and 20 m $\Delta\tilde{y}$ alongshore resolution respectively. Additionally, subaerial only maps were constructed from subaeral surveys and the subaerial portions of full surveys at all sites, binned with 20 m $\Delta\tilde{y}$ alongshore resolution. The spatially varying unnourished times mean was then removed from the binned observations,

$$d' = d - < d > \tag{A.1}$$

where the data fluctuation is a combination of the true signal fluctuation, s, and noise, ε

$$d' = s' + \varepsilon. \tag{A.2}$$

We used $\varepsilon = 2$ cm, the mean standard error in each grid cell. This value is sometimes higher (~7 cm), however, over canyon, reef, or shoal. These binned fluctuations were then smoothed, and empty grid cells filled with a simple mapping scheme. Each mapped fluctuation grid point, m', is a linear combination of the observed data fluctuations

$$m' = a^T d'. \tag{A.3}$$

where the mean square error, $< e^2 >$,

$$< e^2 > = < (m' - s')^2 > \tag{A.4}$$

$$= a^T < d'd'^T > a - 2 < d's' > a + < s'^2 > \tag{A.5}$$

is minimized with gain,

$$a = < d'd'^T >^{-1} < d's' > . \tag{A.6}$$

Covariance matrices are often modeled by a functional fit to the observed autocovariance, where noise is assumed uncorrelated with the signal and between gridpoints (Bretherton et al., 1976),

$$< d'd'^{T} >=< s's'^{T} > + < \epsilon^2 > . \tag{A.7}$$

Considerable effort to model the spatially complex patterns of the observed autocovariance did not significantly improve results compared with a simple Gaussian

$$< s's'^{T} >=< s'^2 > exp\left(- (\Delta\tilde{y}/L\tilde{y})^2 - (\Delta\tilde{x}/L\tilde{x})^2 \right), \tag{A.8}$$

$L\tilde{y} = 200$ m and $L\tilde{x} = 30$ cm (mean vertical) are chosen to fill typical survey gaps with minimal smoothing (similar to Plant et al. (1999)). Grid points are retained only if the normalized mean square error, NMSE $=< e^2 > / < s'^2 >$ is < 0.2. These maps are used to estimate the minimum observed surface over the entire record (Figure A1).

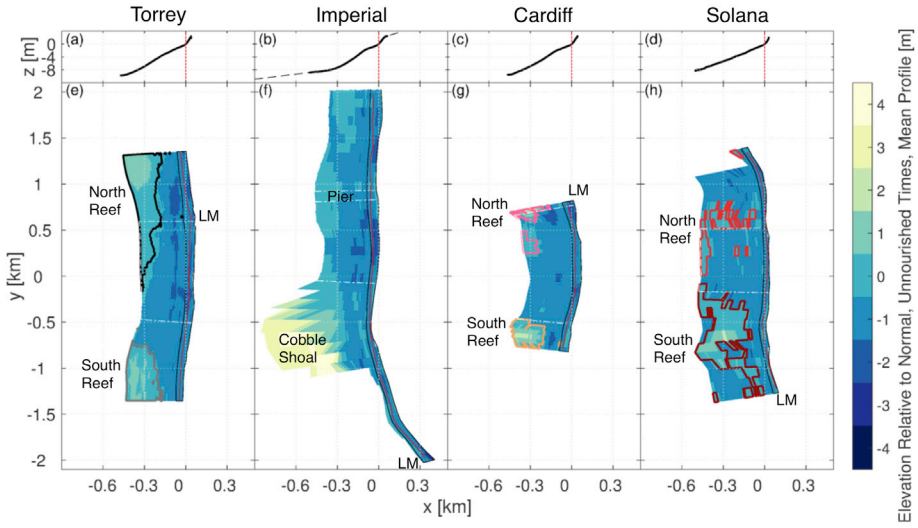

Fig. A1. Left to right, Torrey Pines, Imperial, Cardiff, and Solana Beach. (a-d) Alongshore averaged, unnourished times mean cross-shore profile from "normal" regions outlined with thin white dashed line in (e-h). (e-h) Minimum surface (color bar, Appendix A) plotted relative to profiles in (a-d). "Normal" regions had correlated elevation fluctuations in the alongshore direction (not shown) and contained minimal hard substrate as identified by sidescan sonar (panel a, Figs. 7, 10, Figs. S5 and S6) (Moffatt and Nichol, 2009). The mean horizontal location of MSL during unnourished times (thin red line, e-h), defines the origin (red dotted line a-d) of each profile used to anchor the calculations along a curving coastline. Sandy beaches (blues, e-h) erode below the average normal profiles in (a-d). Reefs and a cobble shoal have a weaker minimum (yellow/-green) than the surrounding area. Areas with minimum surface $> -$ 30cm relative to the profiles in (a-d) and outside the subaerial zone are labeled, and reefs (Fig. 11) are outlined. LM indicates lagoon mouth.

Appendix B. Volume error estimates

A GPS bias of 3 cm (a typical observed value at known benchmarks checked during every survey at Cardiff and Imperial Beach) over the entire domain was assumed as the error of long-period GPS noise (Borsa et al., 2007). Offshore bathymetry is measured using the travel time of acoustic pings from a GPS equipped jet ski to the sea floor and back, using the speed of sound measured at the surface. Four-months of summer temperature stratification (June–Sept 2012) measured at the Scripps Pier shows that the assumption of a well-mixed water column underestimates the depth by at most a few cm. The largest errors are in the deepest depth (8 m), and the sonar bias contribution over the survey area is <1 cm (smaller than GPS and vehicle orientation errors).

At Cardiff Beach, volume estimates from relatively high resolution surveys (50 m alongshore spacing) were compared to volumes from the same surveys decimated to 100 m spacing. At the other sites, high resolution surveys are only available over small areas, so 100 m surveys are compared with surveys decimated to 200 m resolution. At each beach, the maximum difference between volumes was used as the interpolation error. Nourished and unnourished times were treated separately. Surveys spaced close in time at Torrey Pines (2001–2002, Fig. 10c), and at Cardiff during the winters of 2010–11 and 2012-13 (Fig. S5c), suggest the quarterly sampling usually captures much of the temporal variability.

Appendix C. Supplementary data

Supplementary data related to this article can be found at https://doi.org/10.1016/j.coastaleng.2018.02.003.

References

Alexandrakis, G., Manasakis, C., Kampanis, N.A., 2015. Valuating the effects of beach erosion to tourism revenue. A management perspective. Ocean Coast Manag. 111, 1–11.
Anfuso, G., Benavente, J., Gracia, F.J., 2001. Morphodynamic responses of nourished beaches in SW Spain. J. Coast Conserv. 7 (1), 71–80.
Baker, D., 2016. Tijuana River Reopened after Blockage Kills Sharks, Floods Streets. San Diego Union Tribune, 12 April 2016.
Benedet, L., Finkl, C.W., Hartog, W.M., 2007. Processes controlling development of erosional hot spots on a beach nourishment project. J. Coast Res. 33–48.
Bocamazo, L.M., Grosskopf, W.G., Buonuiato, F.S., 2011. Beach nourishment, shoreline change, and dune growth at Westhampton Beach, New York, 1996-2009. J. Coast Res. 181–191.
Borsa, A.A., Minster, J.B., Bills, B.G., Fricker, H.A., 2007. Modeling long-period noise in kinematic GPS applications. J. Geodes. 81 (2), 157–170.
Bretherton, F.P., Davis, R.E., Fandry, C.B., 1976, July. A technique for objective analysis and design of oceanographic experiments applied to MODE-73. Deep-Sea Res. Oceanogr. Abstr. 23 (7), 559–582.
Browder, A.E., Dean, R.G., 2000. Monitoring and comparison to predictive models of the Perdido Key beach nourishment project, Florida, USA. Coastal Eng. 39 (2), 173–191.
Castelle, B., Turner, I.L., Bertin, X., Tomlinson, R., 2009. Beach nourishments at Coolangatta Bay over the period 1987-2005: impacts and lessons. Coastal Eng. 56 (9), 940–950.
CERC, 1984. Shore Protection Manual. U.S. Army Coastal Engineering Research Center, Corps of Engineers, Vicksburg, Mississippi.
Clayton, T., 1991. Beach replenishment activities on US continental pacific coast. J. Coast Res. 1195–1210.
Coastal Frontiers, 2005. 2004 regional Beach Monitoring Program, Report. San Diego Association of Governments, 401 B Street, Suite 800, San Diego, CA 92101, USA.
Coastal Frontiers, 2015. 2014 regional Beach Monitoring Program, Report. San Diego Association of Governments, 401 B Street, Suite 800, San Diego, CA 92101, USA.

Cooke, B.C., Jones, A.R., Goodwin, I.D., Bishop, M.J., 2012. Nourishment practices on Australian sandy beaches: a review. J. Environ. Manag. 113, 319–327.
Cooper, N.J., 1998. Assessment and prediction of Poole Bay (UK) sand replenishment schemes: application of data to Fuhrboter and Verhagen Models. J. Coast Res. 353–359.
Davis Jr., R.A., Wang, P., Silverman, B.R., 2000. Comparison of the performance of three adjacent and differently constructed beach nourishment projects on the Gulf Peninsula of Florida. J. Coast Res. 396–407.
de Schipper, M.A., de Vries, S., Ruessink, G., de Zeeuw, R.C., Rutten, J., van Gelder-Maas, C., Stive, M.J., 2016. Initial spreading of a mega feeder nourishment: observations of the sand engine pilot project. Coastal Eng. 111, 23–38.
Dean, R.G., Yoo, C.H., 1992. Beach-nourishment performance predictions. J. Waterw. Port, Coast. Ocean Eng. 118 (6), 567–586.
Dean, R.G., 2002. Beach nourishment: Theory and Practice, vol. 18. World Scientific Publishing Co Inc.
Diehl, P., 2015. Solana Beach, Encinitas OK Sand Replenishment. San Diego Union Tribune, 15 Oct 2015.
Elko, N.A., Wang, P., 2007. Immediate profile and planform evolution of a beach nourishment project with hurricane influences. Coastal Eng. 54 (1), 49–66.
Gares, P.A., Wang, Y., White, S.A., 2006. Using LIDAR to monitor a beach nourishment project at Wrightsville beach, North Carolina, USA. J. Coast Res. 1206–1219.
Griggs, G., Kinsman, N., 2016. Beach widths, cliff slopes, and artificial nourishment along the California coast. Shore Beach 84 (1).
Group Delta Consultants, 1998. Shoreline Erosion Study North Solana Beach, California Report. Solana Beach Coastal Preservation Association, 219 Pacific Avenue Solana Beach, California 92075, USA.
Haddad, T.C., Pilkey, O.H., 1998. Summary of the New England beach nourishment experience (1935-1996). J. Coast Res. 1395–1404.
Hanson, H., Brampton, A., Capobianco, M., Dette, H., Hamm, L., Laustrup, C., Lechuga, A., Spanhoff, R., 2002. Beach nourishment projects, practices, and objectives - a European overview. Coastal Eng. 47 (2), 81–111.
Hargrove, D., 2015. What Happens when You Bring Sand to the Beach: IB Homeowners Claim SANDAG Created Flood Hazard. San Diego Reader, 24 Jan 2015.
Kuang, C., Pan, Y., Zhang, Y., Liu, S., Yang, Y., Zhang, J., Dong, P., 2011. Performance evaluation of a beach nourishment project at West Beach in Beidaihe, China. J. Coast Res. 27 (4), 769–783.
Longuet-Higgins, M.S., 1970. Longshore currents generated by obliquely incident sea waves, 1. J. Geophys. Res. 75 (33), 6778–6789.
Ludka, B.C., Gallien, T., Crosby, S., Guza, R.T., 2016. Mid-El Niño erosion at nourished and unnourished southern California beaches. Geophys. Res. Lett. 42 (9), 4510–4516.
Ludka, B., Guza, R., O'Reilly, W., Yates, M., 2015. Field evidence of beach profile evolution toward equilibrium. J. Geophys. Res.: Oceans 120 (11), 7574–7597.
Luo, S., Cai, F., Liu, H., Lei, G., Qi, H., Su, X., 2015. Adaptive measures adopted for risk reduction of coastal erosion in the People's Republic of China. Ocean Coast Manag. 103, 134–145.
Moffatt, Nichol, 2009. Coastal Regional Sediment Management Plan for the San Diego Region, Tech. rep., Prepared for the SANDAG and California Coastal Sediment Management Workgroup, 3780 Kilroy Airport Way, Suite 600, Long Beach, California 90806.
Moffatt, Nichol, 2013. Regional Beach Sand Project II Plans, Report. San Diego Association of Governments, 401 B Street, Suite 800, San Diego, CA 92101, USA.
McGranahan, G., Balk, D., Anderson, B., 2007. The rising tide: assessing the risks of climate change and human settlements in low elevation coastal zones. Environ. Urbanization 19 (1), 17–37.
O'Reilly, W.C., Guza, R.T., 1998. Assimilating coastal wave observations in regional swell predictions. Part I: inverse methods. J. Phys. Oceanogr. 28 (4), 679–691.
O'Reilly, W.C., Olfe, C.B., Thomas, J., Seymour, R.J., Guza, R.T., 2016. The California coastal wave monitoring and prediction system. Coastal Eng. 116, 118–132.
Park, J.Y., Gayes, P.T., Wells, J.T., 2009. Monitoring beach renourishment along the sediment-starved shoreline of Grand Strand, South Carolina. J. Coast Res. 336–349.
Pelnard-Considére, R., 1956. Essai de theorie de l'evolution des formes de rivage en plages de sable et de galets. In: 4th Journees de l'Hydraulique, Les Energies de la Mer, Paris, vols. III-1. Soc. de Hydrotech. de Fr., Paris, p. 289298.
Pendleton, L., Mohn, C., Vaughn, R.K., King, P., Zoulas, J.G., 2011. Size matters: the economic value of beach erosion and nourishment in Southern California. Contemp. Econ. Pol. 30 (2), 223–237.
Plant, N.G., Holman, R.A., Freilich, M.H., Birkemeier, W.A., 1999. A simple model for interannual sandbar behavior. J. Geophys. Res. 104 (C7), 15,755.
Roberts, T.M., Wang, P., 2012. Four-year performance and associated controlling factors of several beach nourishment projects along three adjacent barrier islands, west-central Florida, USA. Coastal Eng. 70, 21–39.
Roelvink, D., 2015. Addressing local and global sediment imbalances: coastal sediments as rare minerals. In: The Proceedings of the Coastal Sediments 2015.
Seymour, R., Guza, R.T., O'Reilly, W., Elgar, S., 2005. Rapid erosion of a small southern California beach fill. Coastal Eng. 52 (2), 151–158.
Stocker, T.F., Qin, D., Plattner, G.K., Tignor, M., Allen, S.K., Boschung, J., Nauels, A., Xia, Y., Bex, V., Midgley, P.M., 2013. IPCC, 2013: Climate Change 2013: the Physical Science Basis. Contribution of Working Group I to the Fifth Assessment Report of the Intergovernmental Panel on Climate Change. Cambridge University Press, Cambridge, United Kingdom and New York, NY, USA.
Thornton, E.B., Guza, R.T., 1986. Surf zone longshore currents and random waves: field data and models. J. Phys. Oceanogr. 16 (7), 1165–1178.
Trembanis, A.C., Pilkey, O.H., 1998. Summary of beach nourishment along the US Gulf of Mexico shoreline. J. Coast Res. 407–417.
Valverde, H.R., Trembanis, A.C., Pilkey, O.H., 1999. Summary of beach nourishment episodes on the US east coast barrier islands. J. Coast Res. 1100–1118.
Wooldridge, T., Heather, H.J., Kohn, J.R., 2016. Effects of beach replenishment on intertidal invertebrates: a 15-month, eight beach study. Estuar. Coast Shelf Sci. 175 (1), 24–33.
WorleyParsons, 2013. Assessing the Value of Coastal Resources in Victoria, Report. Level 6, 8 Nicholson St, East Melbourne VIC 3002, Australia.
Wright, L.D., Short, A.D., 1984. Morphodynamic variability of surf zones and beaches: a synthesis. Mar. Geol. 56 (1), 93–118.
Wright, L.D., Short, A.D., Green, M.O., 1985. Short-term changes in the morphodynamic states of beaches and surf zones: an empirical predictive model. Mar. Geol. 62 (3–4), 339–364.
Yates, M., Guza, R., O'reilly, W., Seymour, R., 2009. Seasonal persistence of a small southern California beach fill. Coastal Eng. 56 (5), 559–564.